AIAA 2004-3516

On Nonlinear Combustion Instability in Liquid Propellant Rocket Engines

G. A. Flandro and J. Majdalani
Advanced Theoretical Research Center
University of Tennessee Space Institute
Tullahoma, TN 37388

J. D. Sims
NASA Marshall Space Flight Center
Huntsville, AL 35806

40th AIAA/ASME/SAE/ASEE Joint Propulsion Conference and Exhibit
11–14 July 2004
Fort Lauderdale, FL

40th AIAA/ASME/SAE/ASEE Joint Propulsion Conference and Exhibit
11-14 July 2004, Fort Lauderdale, Florida

AIAA 2004-3516

On Nonlinear Combustion Instability in Liquid Propellant Rocket Engines

Gary A. Flandro* and Joseph Majdalani†
University of Tennessee Space Institute, Tullahoma, TN 37388
and
Joseph D. Sims‡
NASA Marshall Space Flight Center, Huntsville, AL 35806

All liquid propellant rocket instability theories in current use have limited value in the predictive sense and serve mainly to correlate available experimental data. The well-known *n*-τ model first introduced by Crocco and Cheng in 1956[1] is still resorted to as the primary analytical tool of this type. A multitude of attempts to establish practical analytical methods have achieved only limited success.[2-7] These methods usually produce stability boundary maps that are difficult to use in making critical design decisions in new engine development programs. Recent progress in understanding the mechanisms of combustion instability in solid propellant rockets[8-11] establishes a firm foundation for a new approach to prediction, diagnosis, and correction of the closely related problems in liquid engine instability. For predictive tools to be useful in the engine design process, they must have the capability to accurately determine: 1) time evolution of the pressure oscillations and limit amplitude, 2) critical triggering pulse amplitude, 3) unsteady heat transfer rates at injector surfaces and chamber walls, and 4) mean pressure DC shift. The method described in this paper relates these critical engine characteristics directly to system design parameters. Inclusion of mechanisms such as wave steepening, vorticity production and transport, and unsteady detonation wave phenomena greatly enhance the representation of key features of engine chamber oscillatory behavior. In this study, the basic theoretical model is described and preliminary computations are compared to experimental data. A plan to develop the new predictive method into a comprehensive analysis tool is also presented.

Nomenclature

A_p	= unsteady pressure amplitude
a_0	= mean speed of sound
e	= oscillatory energy density
$\bar{E}$	= time-averaged oscillatory system energy
E_m^2	= normalization constant for mode *m*
k_m	= wave number for axial mode *m*
L	= chamber length
m	= mode number
$\bar{M}$	= reference chamber Mach number
$\boldsymbol{n}$	= outward pointing unit normal vector
p	= pressure
$\bar{P}$	= mean chamber pressure
r	= radial position
R	= chamber radius
S	= Strouhal number, $k_m / \bar{M}_b$
t	= time
$\boldsymbol{u}$	= oscillatory velocity vector
U_r, U_z	= mean flow velocity component
z	= axial position
α	= growth rate (dimensional, $\sec^{-1}$)
δ	= reciprocal of square root of the acoustic Reynolds number, $\sqrt{\nu/(a_0 R)}$
δ_d	= compressible viscous length, $\delta\sqrt{(\eta/\mu+\frac{4}{3})}$
ε	= wave amplitude, $A_p/(\gamma p_0)$
γ	= ratio of specific heats
η	= second coefficient of viscosity, $-\frac{2}{3}\mu$
ν	= kinematic viscosity, μ/ρ
ρ	= density
ω	= unsteady vorticity magnitude
Ω	= mean vorticity magnitude

Subscripts

b	= combustion zone
m	= specific to a given mode number

*Boling Chair Professor of Excellence in Propulsion, Department of Mechanical, Aerospace and Biomedical Engineering. Associate Fellow AIAA.

†Jack D. Whitfield Professor of High Speed Flows, Department of Mechanical, Aerospace and Biomedical Engineering. Member AIAA.

‡Liquid Propulsion Systems Engineer, Combustion Devices Team. Member AIAA.

Superscripts

*	= dimensional quantity
~	= vortical (rotational) part
^	= acoustic (irrotational) part
($\underline{r}$), (i)	= part of a complex variable
	= mean quantity

I. Introduction

THE combustion instability problem is staggeringly complex. It involves many physical and chemical mechanisms that are not yet fully understood. This has resulted in an engine design process that, for the most part, simply ignores the possibility of combustion instability until it appears, unexpectedly, at the testing stage of a new system. Unfortunately, it is expensive and time consuming to correct oscillatory behavior when it is already encountered. Although there exists a set of proven corrective procedures, they must still be applied in an *ad hoc* fashion, and without full understanding of the physical mechanisms involved. In other words, it is still a "cut-and-try" effort that has evolved from difficulties such as those experienced in Saturn V (F-1) engine development.[5] In the present environment, such an occurrence would doubtless spell the cancellation of a new engine development program. In short, the ability to anticipate combustion instability problems at the design stage does not presently exist in practical form.

Nevertheless, when the key findings of many investigators collected over a period of several decades are carefully engaged and merged, a global picture of the combustion instability phenomenon emerges. It becomes clear that useful design tools can be devised that incorporate the seemingly divergent information that has resulted from these research programs. This has been recently demonstrated in similar problems encountered in solid propellant rocket development.[11-13] The purpose of this paper is to describe methods for building this information into a new analytical model for predicting, diagnosing, and correcting problems of combustion instability in liquid propellant engines.

For any such tool to be of practical use, it must address many key design-related aspects of combustion instability. Maps of stability boundaries or linear growth rates are of very limited use in this regard. The engine design team must have powerful tools that relate possible pressure oscillation limit amplitudes, triggering pressures, and heat transfer rates to design features and engine configurations. With these tools at hand, design tradeoffs can be accomplished to minimize the possibility of ensuing stability problems. The same analytical tools can provide potential cost, system weight, and development time benefits, since they avoid the usual blind application of conventional acoustic baffles, resonator cavities, liners, and the like, that are often included without full justification or functional understanding.

In this paper we describe in detail the required physical models and their implementation. Examples are presented demonstrating the capability to represent the key elements of the combustion instability problem. These include:

- steep-fronted, shocked pressure waves,
- effects of rotational flow corrections,
- comprehensive combustion coupling including detonation wave phenomena, and
- surface effects including heat transfer computations.

Naturally, construction of a practical algorithm for liquid rocket engine combustion oscillations can greatly benefit from the pitfalls and successes experienced in parallel developments in the solid motor arena. In what follows, this experience is used to full advantage.

II. Analytical Foundations

Earlier analyses were, for the most part, built upon the assumption of a system of irrotational acoustic waves. Experimental data will be reviewed showing the limitations imposed by this approach. Careless application of simplifying assumptions often leads to incorrect or incomplete results. The acoustic wave assumption is motivated by the observation that reported oscillatory frequencies are often close to those corresponding to the acoustic modes of the combustion chamber. However, adopting an acoustic basis alone results in the inability to accommodate correct boundary conditions (such as the no-slip condition at chamber boundaries) and the loss of important flow features, such as unsteady vorticity, that can have major impact on the validity of the results. It is also difficult to properly treat finite amplitude waves using a purely acoustic model. There is overwhelming evidence that the high-amplitude wave systems in unstable rockets are more akin to traveling shock fronts.[14-17] Early efforts were made to account for steepened wave effects,[6-7] but the analytical methods applied did not lead to practical solutions. These were mainly applications of the method of characteristics that did not lend themselves well to generalized computational techniques of the kind needed for a practical stability assessment algorithm.

A. Experience with Solid Propellant Motors

The well-known failure of predictive algorithms in solid rocket analysis is largely the result of neglect in key features of the unsteady flow of combustion products. In particular, one must account for effects of

vorticity production and propagation, and for the tendency of initially weak (essentially acoustic) waves to steepen into shock-like motion. When such waves interact with a combustible mixture of injectants, the possibility of unsteady detonation waves must also be addressed. Very significant improvement in predictive capability results from inclusion of these features which, until recently, were not included in either liquid or solid motor analyses.

Solid propellant rocket motor analysis as applied in the SSP (Standard Stability Prediction) computer program, implements Culick's fundamentally irrotational acoustics.[2-4,8-11,18-22] While the general Culick approach introduces a more complete formulation than similar algorithms in the accepted liquid rocket toolkit, it does not yield satisfactory predictive outcome. This is partly the result of the assumption that the wave motions are strictly acoustic (irrotational) in nature. Recent work by the writers of the present paper has focused on improving SSP by inclusion of important mechanisms such as vorticity generation and shock wave interactions. Much of the recent progress in solid motor analysis leads directly to similar improvements in handling the liquid rocket instability problem.

It may be safe to say that Culick's papers on combustion instability[19,20,23-25] stand behind most stability prediction methods now in use.[26,27] However, in order to make progress, the limitations of his framework must be well understood; his are based on three fundamental assumptions:

- the low speed mean flow is subject to small amplitude pressure fluctuations,
- the reacting surface layer is thin and permeable, thus permitting mass addition, and
- the oscillatory flowfield is driven by chamber acoustic modes.

The first assumption enables us to linearize the problem using a doubly perturbated methodology that expands the governing equations asymptotically both in the wave amplitude and the surface Mach number of the mean injected flow. The second idea of a thin permeable sheet allows the complex surface reaction effects, including combustion and pressure coupling, to be expressible via simple acoustic admittance boundary conditions imposed at the chamber surfaces. The last assumption, namely that of an acoustic representation of the unsteady flowfield, oversimplifies the time-dependent model by suppressing all unsteady rotational flow effects at the leading order. Considering that the acoustic representation is strictly irrotational, concern for this deficiency was partially addressed by Culick in a paper in which he introduced a revised rotational mean flow model.[24] However, his analysis introduced vortical effects as a secondary correction, thus limiting their contribution at leading order; in the process, the no slip boundary, which requires both rotational and irrotational wave interactions at the same order, could not be satisfied. Unsurprisingly, stability calculations based on this revised mean flow representation produced no significant changes in the system stability characteristics. On this basis, it has since been generally assumed that all vorticity (rotational flow effects), including the unsteady part, can have no measurable influence on combustion instability growth rate calculations. In practice, however, this irrotational hypothesis has proven to be a misconception.

B. Rotational Flow Effects

Considerable progress has been made in the last decade in understanding both the precise source of the vorticity and the resulting changes in the oscillatory flowfield. Analytical,[10,28-35] numerical,[36-41] and experimental investigations[42-45] have demonstrated that rotational flow effects play an important role in the unsteady gas motions in solid rocket motors. Much effort has been directed to constructing the required corrections to the acoustic model. This has culminated in a newer and more concrete picture of the unsteady motions that agrees more convincingly with experimental measurements,[10,28,29] as well as numerical simulations.[30]

It may be worthy to note that these models have also been implemented in carrying out three-dimensional system stability calculations,[10,28] in a first attempt to account for rotational flow effects and correct the acoustic instability algorithm. In this process, one discovers the origin and the three-dimensional form of the *flow-turning* correction; related terms appear that are not accounted for in the SSP algorithm. In particular, a rotational correction term is identified that cancels the flow-turning energy loss in a full-length cylindrical grain. However, all of these results must now be questioned because they are founded on an incomplete representation of the system energy balance.

Culick's stability estimation procedure is based on calculating the exponential growth (or decay) of an irrotational acoustic wave; the results are equivalent to energy balance models used earlier by Cantrell and Hart.[46] In all of these calculations the system energy is represented by the classical Kirchoff (acoustic) energy density. Consequently, it does not represent the *full* unsteady field, which must include both acoustic and rotational flow effects. Failure to do so will lead to the dismissal of the kinetic energy carried by the vorticity waves. It is readily demonstrated that the actual average unsteady energy contained in the system at a given time is about 25% larger than the acoustic energy

alone.[11] At the outset, representation of the energy sources and sinks that determine the stability characteristics of the motor chamber must also be modified. However, attempts to correct the acoustic growth rate model by retention of rotational flow source terms only,[10,28] preclude a full representation of the effects of vorticity generation and coupling.

In liquid engines, the main role played by the rotational flow interactions is in controlling boundary conditions at the chamber walls, especially, at the injector boundaries. Vorticity is created in the case of waves traveling parallel to the injection interface because such waves (tangential modes, for example) represent unsteady pressure gradients across the incoming quasi-steady flow streamlines. This vorticity is propagated into the chamber mainly by convection, and it has important implications in terms of engine stability. These effects will be examined carefully as we carry out the stability analyses in the next section of the paper.

C. Nonlinear Effects

The effects of nonlinear interactions play a major role in controlling all important attributes of nonlinear pressure oscillations in liquid engine combustion chambers. In this context, linearized models are of little value. Of crucial importance is the modeling of the time history of the oscillations and their limiting amplitude, in addition to the triggering amplitudes at which an otherwise stable engine is caused to transition to violent oscillations. Pulsing of this sort can occur from random "popping" and other natural disturbances, so it is important to characterize this aspect of engine behavior.

It is well-known that shock waves are a major nonlinear attribute of axial mode oscillations in solid rockets.[47-50] Current work with liquid engine preburners shows similar longitudinal mode shocks.[51] In what follows, we plan to establish that similar effects are associated with transverse modes despite widely-held contrary views.[52]

D. Transverse Mode Shock Waves

Study of the Saturn V first stage F-1 engine development stability problems[53] gives much guidance in the modeling requirements addressed in this paper. Examination of the oscillatory pressure data for this engine (see Fig. 1) indicates the presence of steep fronted, shock-like waves. This is such a familiar case that we will omit its detailed account here. Instead, we choose to emphasize related information that has been apparently overlooked by the combustion instability research community. In particular, we focus in this subsection on the strong evidence for shock and detonation wave effects as an integral feature of liquid rocket instability. We thus return to the course of the F-1 investigation in the late 1960's; specifically, we refer the reader to the fundamental research conducted at the Caltech Jet Propulsion Laboratory by Clayton and his co-workers. These have gathered invaluable data using a highly instrumented liquid rocket engine illustrated in Fig. 2.[14-17,54] This particular device allows detailed measurement of the time-dependent pressure waves throughout the engine cavity; it also included motion-picture recording of events within the chamber by means of a protected camera placed just outside the nozzle throat (sans exit cone).[15,54] The investigators describes the unsteady flowfield as a "traveling detonation wave." The presence of steep high-amplitude wave fronts is clearly depicted in the pressure traces measured near the injector face; in the interest of clarity, these are reproduced in Fig. 3.

The waves have been identified by their dominant frequency component which corresponds to the first tangential acoustic mode. This mode is often associated with the most destructive forms of liquid rocket instability. Although the waveform is steep fronted, it is basically a "shocked" acoustic wave of very large amplitude (on the acoustic scale). Figure 4 shows how the wave energy is distributed axially in the engine. This data is secured using an ablatively cooled Kistler pressure probe that could be accurately placed laterally and axially within the engine. Notice that the kinetic

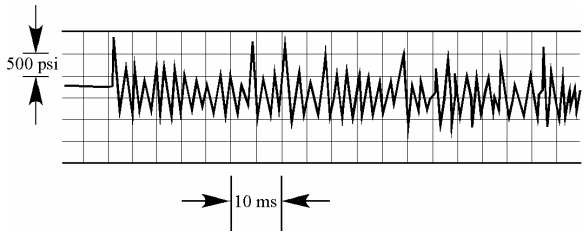

Fig. 1 Evidence of clearly visible shock waves in the F-1 pressure trace.[5,53]

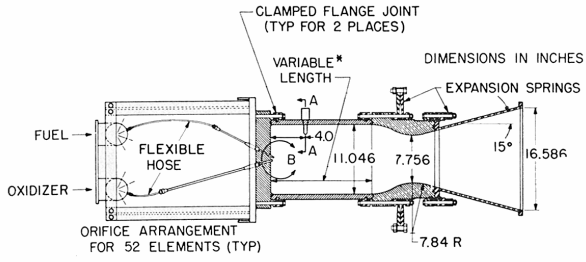

Fig. 2 JPL's 20k-lbf-thrust rocket engine.[17]

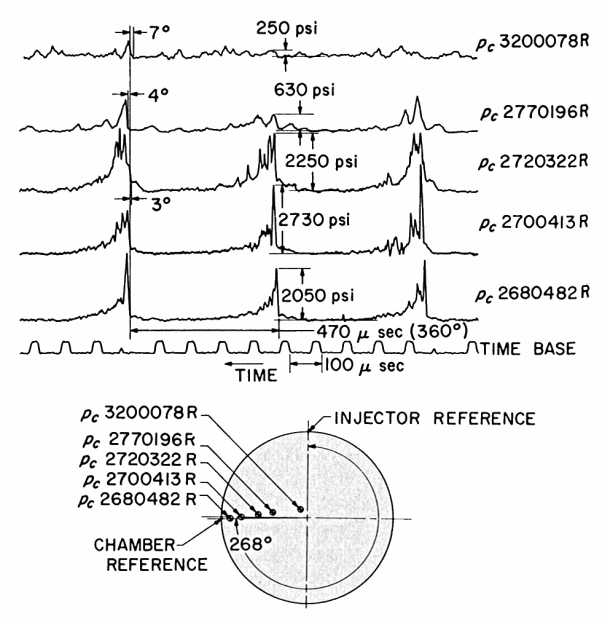

Fig. 3 Evidence of shock waves in JPL's 20k-lbf-thrust rocket engine.[17]

energy associated with the wave is strongest near the chamber wall, and is barely discernible in the nozzle entrance. This provides direct verification of modeling assumptions routinely used in handling the unsteady nozzle boundary conditions. The records were obtained during resonant combustion initiated by a 25 msec bomb pulse.

III. Formulation

In this section we briefly discuss what is needed from the theoretical standpoint to provide a useful analytical framework for combustion instability. It is necessary to accommodate the features we have identified as key elements in a judicious physical representation. We must discard models based strictly on the acoustic point of view. Nonlinear energy losses in steep wave fronts and energy flow to the wave structure from combustion must be involved. It is also necessary to provide a framework that can ultimately capture effects of mixing, vaporization, and other two phase flow effects. These elements will be described in outline form, specifically, as placeholders that will require later elaboration. The most effective method for incorporating this large array of physical/chemical interactions is by using a global nonlinear energy balance. Methods based on the usual perturbed acoustic wave equation *cannot* properly account for the many interactions that must be resolved.

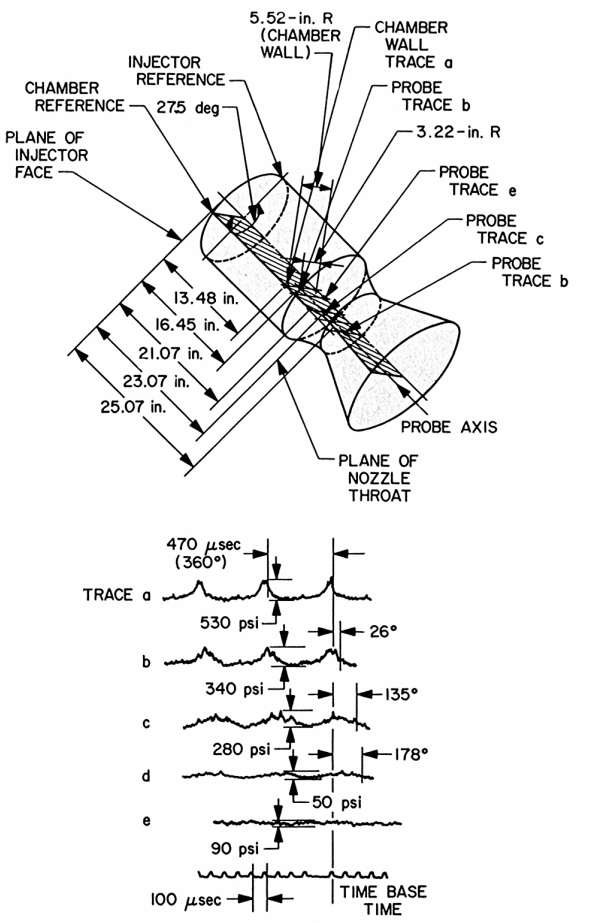

Fig. 4 Axial amplitude distribution.[17]

A. Mathematical Strategy

Since a pivotal aspect here is the handling of steep fronted waves, it is necessary to carefully lay out a solution technique that will lead to a practical predictive algorithm. To make the mathematical problem tractable, we choose to avoid the fashionable numerical strategies such as the method of characteristics or a full CFD treatment of the problem. Either of these techniques would likely fail in the problem we are attempting to solve here. What is required is an approach that bridges the gap between the earlier perturbation techniques that limit the solutions to linear gas motions, and other *ad hoc* methods such as those introduced by Culick to study nonlinear features of combustion instability.[3,21,55] In the latter, Culick and his co-workers model the steepening process in which energy cascades by nonlinear mode coupling from low frequency to higher frequency spectral components.

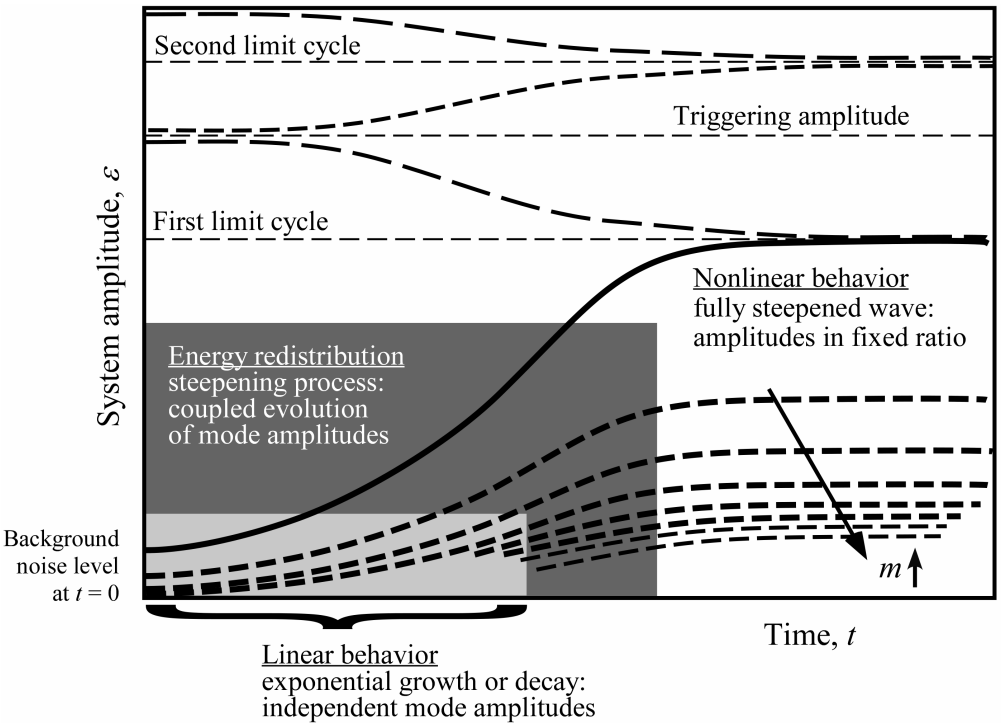

Fig. 5 Time evolution of system amplitude.

In the problem of central interest here, we are not concerned with the steepening process, *per se*; rather, we wish to understand the gas motions in the fully steepened state. Figure 5 illustrates several aspects of the problem we must solve. This diagram furnishes in schematic form all features of combustion instability that appear experimentally. Furthermore, it provides a useful way to categorize the various analytical methods by which we attempt to understand this very complicated physical problem. For example, if the waves grow from noise in the linear fashion, it can be seen that the motion is linear and each acoustic mode grows individually according to the balance of energy gains and losses peculiar to that operating frequency. In general, the lowest order mode grows most rapidly because it requires less energy to excite. As the oscillations grow to a finite amplitude, nonlinear effects appear and there is a phase in which energy is redistributed from lower to higher modal components; it is this cascading process that is described in Culick's nonlinear model.

As the wave steepens, the relative amplitudes of the constituent acoustic modes reach a frozen state corresponding to shock-like behavior. This is the fully nonlinear state illustrated in the right section of Fig. 5. In pulse testing of motors, the steepening process is almost instantaneous. For example, Brownlee[47] notes that when the pulse was fired, "…the injected flow disturbance traversed the length of the motor, partially reflected at the nozzle end, and became a steep-fronted shock-like wave in one cycle." Thus, in modeling such effects, it is unnecessary to trace the full steepening process. The relative wave amplitudes are readily estimated from a large database of experimental data. It is readily established that precise knowledge of the relative amplitudes is not necessary to achieve an accurate estimate of the limit cycle and triggering amplitudes.

To alleviate current deficiencies in predictive theory, we must formulate a mathematical strategy that yields the key information, namely, the limit amplitude reached by the system in the fully steepened state. This is the information required by the engine designer in assessing potential vibration levels, and as we will show, the severity of heat loads and force levels on fragile injector components.

The key to simplifying the nonlinear problem is to assume that the fully steepened *traveling* wave is a composite of the chamber normal modes:

$$p(\boldsymbol{r},t) = \varepsilon(t)\sum_{m=1}^{\infty} A_m(t)\psi_m(\boldsymbol{r}) \qquad (1)$$

where $\varepsilon(t)$ is the instantaneous amplitude. This is a proven simplifying strategy[48,49] that conforms well to all experimental features that must be built into our solution algorithm.

B. Notation

The following dimensionless variables will be used (star * denotes dimensional quantities; subscript 0 indicates quiescent chamber reference conditions):

$$\begin{cases} p = p^*/P_0 \\ \rho = \rho^*/\rho_0 \\ T = T^*/T_0 \\ \boldsymbol{u} = \boldsymbol{u}^*/a_0 \\ \boldsymbol{r} = \boldsymbol{r}^*/L \end{cases} \qquad \begin{cases} \boldsymbol{F} = \boldsymbol{F}^*/\left(\rho_0 a_0^2/L\right) \\ t = t^*/\left(L/a_0\right) \\ \boldsymbol{\omega} = \boldsymbol{\omega}^*/\left(a_0/L\right) \\ e = e^*/a_0^2 \end{cases} \tag{2}$$

where $\boldsymbol{F}$ is a body force and e is the specific internal energy. The dimensionless governing equations are:

Continuity

$$\frac{\partial \rho}{\partial t} + \nabla \cdot \left(\rho \boldsymbol{u}\right) = 0 \tag{3}$$

Momentum

$$\rho\left(\frac{\partial \boldsymbol{u}}{\partial t} + \tfrac{1}{2}\nabla \boldsymbol{u}\cdot\boldsymbol{u} - \boldsymbol{u}\times\boldsymbol{\omega}\right) = -\frac{1}{\gamma}\nabla p - \delta^2 \nabla\times\nabla\times\boldsymbol{u} + \delta_d^2 \nabla\left(\nabla\cdot\boldsymbol{u}\right) + \boldsymbol{F} \tag{4}$$

Energy

$$\frac{\partial}{\partial t}\left[\rho\left(e + \tfrac{1}{2}\boldsymbol{u}\cdot\boldsymbol{u}\right)\right] + \nabla\cdot\left[\rho\boldsymbol{u}\left(e + \tfrac{1}{2}\boldsymbol{u}\cdot\boldsymbol{u}\right)\right] = \begin{Bmatrix} \dfrac{\delta^2}{(\gamma-1)Pr}\nabla^2 T - \dfrac{1}{\gamma}\nabla\cdot\left(p\boldsymbol{u}\right) + \rho\boldsymbol{u}\cdot\left(\boldsymbol{u}\times\boldsymbol{\omega}\right) \\ +\boldsymbol{u}\cdot\boldsymbol{F} + \delta^2\left[\boldsymbol{\omega}\cdot\boldsymbol{\omega} - \boldsymbol{u}\cdot\nabla\times\boldsymbol{\omega}\right] \\ +\delta_d^2\left[\left(\nabla\cdot\boldsymbol{u}\right)^2 + \boldsymbol{u}\cdot\nabla\left(\nabla\cdot\boldsymbol{u}\right)\right] - \sum_{i=1}^{N} h_i^0 w_i \end{Bmatrix} \tag{5}$$

Species mass fraction

$$\rho\left[\frac{\partial Y_i}{\partial t} + \boldsymbol{u}\cdot\nabla Y_i\right] - \frac{\delta^2}{Pr}\nabla^2 Y_i = w_i \tag{6}$$

State

$$p = \rho T \tag{7}$$

The Prandtl number Pr and viscous reference lengths (proportional to inverse square root of appropriate Reynolds numbers) appear naturally. These are defined as:

$$\begin{cases} Pr \equiv \dfrac{c_p \mu}{\kappa} \\ \delta^2 = \dfrac{\nu}{a_0 L} \\ \delta_d^2 = \delta^2\left(\eta/\mu + \tfrac{4}{3}\right) \\ \delta_f \equiv \dfrac{\kappa}{\rho_0 c_p V_{ref}} = \dfrac{\kappa}{\rho_0 c_p a_0 M_{ref}} \end{cases} \tag{8}$$

The latter reference length is the characteristic flame length needed in regions dominated by combustion heat release. Other variables needed in modeling chemical reactions are:

$$\begin{cases} w = w^*/\left(\rho_0 a_0/L\right); & \text{reaction rate} \\ h_i^0 = h_i^{0*}/a_0^2; & \text{heat of combustion} \\ Y_i; & \text{mass fraction for species } i \end{cases} \tag{9}$$

C. Decomposing Into Steady and Unsteady Parts

The steady and unsteady parts of the variables are separated in the standard manner by writing

$$\begin{cases} \rho = \bar{\rho} + \rho^{(1)} \\ p = \bar{P} + p^{(1)} \\ T = \bar{T} + T^{(1)} \\ \boldsymbol{u} = \bar{M}_b \boldsymbol{U} + \boldsymbol{u}^{(1)} \\ \boldsymbol{\omega} = \bar{M}_b \nabla\times\boldsymbol{U} + \nabla\times\boldsymbol{u}^{(1)} = \bar{M}_b \boldsymbol{\Omega} + \boldsymbol{\omega}^{(1)} \end{cases} \tag{10}$$

Since the energy balance is the key to understanding the system behavior, it must be judiciously evaluated. In what follows, we will avoid the common simplifying assumptions such as the isentropic flow limitation. We will also include heat transfer and viscosity so that, in effect, we are modeling a wave system composed of superimposed waves of compressibility, vorticity, and entropy.

To start, we define the system energy density as

$$\mathscr{E} \equiv \rho\left(e + \tfrac{1}{2}\boldsymbol{u}\cdot\boldsymbol{u}\right) \tag{11}$$

Then, for a calorically perfect gas, the energy equation becomes

$$\frac{\partial \mathscr{E}}{\partial t} = -\nabla\cdot\left[\rho\boldsymbol{u}\left(\frac{T}{\gamma(\gamma-1)} + \tfrac{1}{2}\boldsymbol{u}\cdot\boldsymbol{u}\right)\right] + \begin{Bmatrix} -\dfrac{1}{\gamma}\nabla\cdot\left(p\boldsymbol{u}\right) + \rho\boldsymbol{u}\cdot\left(\boldsymbol{u}\times\boldsymbol{\omega}\right) \\ +\delta^2\left[\boldsymbol{\omega}\cdot\boldsymbol{\omega} - \boldsymbol{u}\cdot\nabla\times\boldsymbol{\omega}\right] + \dfrac{\delta^2}{(\gamma-1)Pr}\nabla^2 T \\ +\delta_d^2\left[\left(\nabla\cdot\boldsymbol{u}\right)^2 + \boldsymbol{u}\cdot\nabla\left(\nabla\cdot\boldsymbol{u}\right)\right] + \dot{Q} + \boldsymbol{u}\cdot\boldsymbol{F} \end{Bmatrix} \tag{12}$$

where a shorthand notation has been adopted for the heat release in the combustion processes. The body force, $\boldsymbol{F}$, is a placeholder for several two-phase flow effects such as spray atomization, particle-mean flow interactions, etc., that will be treated later. Note that the dilatational viscous force and conduction heat transfer terms are retained. These constitute the source of the nonlinear energy loss in steep wave fronts.

Using Eq. (10), one can expand Eq. (11) to produce the system amplitude relation. To accomplish this, the time-averaged Eq. (12) can be written as

$$2\varepsilon\frac{\mathrm{d}\varepsilon}{\mathrm{d}t}\left\langle \mathscr{E}_2\right\rangle = \left\langle \begin{array}{l} -\nabla\cdot\left\{\rho\boldsymbol{u}\left[\dfrac{T}{\gamma(\gamma-1)}+\tfrac{1}{2}\boldsymbol{u}\cdot\boldsymbol{u}\right]\right\}-\dfrac{1}{\gamma}\nabla\cdot(p\boldsymbol{u})+\rho\boldsymbol{u}\cdot(\boldsymbol{u}\times\boldsymbol{\omega})+\boldsymbol{u}\cdot\boldsymbol{F}+\dot{Q} \\ +\delta^2\left[\boldsymbol{\omega}\cdot\boldsymbol{\omega}-\boldsymbol{u}\cdot\nabla\times\boldsymbol{\omega}\right]+\delta_d^2\boldsymbol{u}\cdot\nabla(\nabla\cdot\boldsymbol{u})+\left[\dfrac{\delta^2}{(\gamma-1)Pr}\nabla^2T+\delta_d^2(\nabla\cdot\boldsymbol{u})^2\right] \end{array}\right\rangle \tag{13}$$

where

$$\left\langle \mathscr{E}_2\right\rangle = \frac{1}{\gamma\overline{P}}\left\langle\left(\frac{p'}{\gamma}\right)^2\right\rangle+\tfrac{1}{2}\overline{\rho}\left\langle\boldsymbol{u}'\cdot\boldsymbol{u}'\right\rangle \tag{14}$$

is the time-averaged oscillatory energy. Note that this quantity consists of a "potential" energy part that is proportional to the pressure fluctuation, and a kinetic part, proportional to the square of the particle velocity. The latter is not the simple acoustic particle velocity; it is the composite of the irrotational and rotational parts needed to satisfy correct boundary conditions at the chamber surfaces.

Equation (14) is similar to the usual Kirchoff reference energy density from classical acoustics:[56]

$$\mathscr{E}_{\text{Kirchoff}} = \tfrac{1}{2}\left[p^{(1)}/\gamma\right]^2+\tfrac{1}{2}\overline{\rho}\boldsymbol{u}^{(1)}\cdot\boldsymbol{u}^{(1)} \tag{15}$$

The differences are largely the result of relaxing the isentropic flow assumption used in deriving Eq. (15).

D. Spatial Averaging

In order to account for the net behavior of the entire system it is now required to integrate the time-averaged energy density over the chamber control volume. As usual, one must define the reference system energy,

$$E^2 \equiv \iiint_V\left\langle \mathscr{E}_2\right\rangle\mathrm{d}V = \iiint_V\left\langle\frac{1}{\gamma\overline{P}}\left(\frac{p'}{\gamma}\right)^2+\tfrac{1}{2}\overline{P}\boldsymbol{u}'\cdot\boldsymbol{u}'\right\rangle\mathrm{d}V \tag{16}$$

then the rate of change of system amplitude can be written in the convenient form

$$\frac{\mathrm{d}\varepsilon}{\mathrm{d}t} = \alpha^{(1)}\varepsilon+\alpha^{(2)}\varepsilon^2+\alpha^{(3)}\varepsilon^3+\cdots \tag{17}$$

where $\alpha^{(1)}$ is the linear growth rate for the composite wave system. This series expression emphasizes the important fact that the nonlinear model is only as reliable as the linear representation of the system.

In many ways, achieving a valid linear model is the most difficult part of the entire problem. It has, in fact, been the downfall of numerous past attempts. Much time and energy have been expended on attempts to correct deficiencies in the linear model by introduction of *ad hoc* fixes that are often based on guesswork, and misinterpretation and/or distortion of experimental evidence. The roadway is strewn with the wreckage of such attempts. We avoid the temptation to dwell on this unhappy aspect of the past. Clearly, the only road to success is to avoid losing any of the crucial physical information that has been so carefully collected in the system energy balance constructed here.

E. Linear Growth Rate

The linear part of Eq. (17) becomes

$$\begin{aligned}\alpha^{(1)} = \frac{1}{2E^2}\Bigg\{&-\overline{M}_b\overline{P}\iint_S\boldsymbol{n}\cdot\left\langle\tfrac{1}{2}\boldsymbol{U}(\boldsymbol{u}'\cdot\boldsymbol{u}')+\boldsymbol{u}'(\boldsymbol{U}\cdot\boldsymbol{u}')\right\rangle\mathrm{d}S \\ &-\frac{1}{\gamma}\iint_S\boldsymbol{n}\cdot\left\langle p'\boldsymbol{u}'\right\rangle\mathrm{d}S-\frac{\overline{M}_b}{\gamma\overline{P}}\iint_S\boldsymbol{n}\cdot\boldsymbol{U}\left\langle(p'/\gamma)^2\right\rangle\mathrm{d}S \\ &+\overline{M}_b\overline{P}\iiint_V\left\langle\boldsymbol{u}'\cdot(\boldsymbol{u}'\times\boldsymbol{\Omega})\right\rangle\mathrm{d}V+\overline{M}_b\overline{P}\iiint_V\boldsymbol{U}\cdot\left\langle\boldsymbol{u}'\times\boldsymbol{\omega}'\right\rangle\mathrm{d}V \\ &+\delta^2\iint_S\boldsymbol{n}\cdot\left\langle\boldsymbol{u}'\times\boldsymbol{\omega}'\right\rangle\mathrm{d}S+\delta_d^2\iiint_V\left\langle\boldsymbol{u}'\cdot\nabla(\nabla\cdot\boldsymbol{u}')\right\rangle\mathrm{d}V \\ &+\iiint_V\left\langle\dot{Q}\right\rangle\mathrm{d}V+\iiint_V\left\langle\boldsymbol{F}\right\rangle\mathrm{d}V\Bigg\}\end{aligned} \tag{18}$$

where only the placeholders for combustion heat release and two-phase flow interactions are displayed. Fortuitously, subsequent evaluation of the volume integrals in Eq. (18) leads to many cancellations. One of these is the Culick flow turning effect, which has been the source of considerable argument, disagreement, and controversy in the solid propellant rocket instability research community. The vanishing of this term is of critical importance because its spurious retention leads to a damping effect which, in most engine evaluations, is as large as other main contributions to the energy balance. An appreciable error in predictive theory will thus ensue from keeping this term. To illustrate the handling of its source integral in Eq. (18), we now (correctly) evaluate the specific term from which flow turning originates:

$$\alpha_4^{(1)} = \frac{\overline{M}_b\overline{P}}{2E^2}\iiint_V\left(\boldsymbol{U}\cdot\left\langle\boldsymbol{u}'\times\boldsymbol{\omega}'\right\rangle+\left\langle\boldsymbol{u}'\cdot\boldsymbol{U}\times\boldsymbol{\omega}'\right\rangle\right)\mathrm{d}V \tag{19}$$

The subscript 4 is an artifact of the numbering system introduced in Ref. (11) for keeping track of the many

linear stability contributions stemming from Eq. (18). Flow turning was first identified by Culick[20,25] in his one-dimensional calculations when attempting to force the satisfaction of the no-slip condition (which could not be accomplished in his three-dimensional model because of the irrotational flow assumption). Flandro[10,11,28,57] later showed that the actual source of the flow turning was the irrotational part of the second term in Eq. (19). None of the earlier stability calculations incorporated all of the rotational terms included in Eq. (19). When *all* of the terms are properly accounted for, then by applying the standard scalar triple product identity

$$\boldsymbol{A}\cdot\left(\boldsymbol{B}\times\boldsymbol{C}\right)=\boldsymbol{B}\cdot\left(\boldsymbol{C}\times\boldsymbol{A}\right) \tag{20}$$

it can be easily proven that

$$\boldsymbol{U}\cdot\left\langle\boldsymbol{u}'\times\boldsymbol{\omega}'\right\rangle+\left\langle\boldsymbol{u}'\cdot\boldsymbol{U}\times\boldsymbol{\omega}'\right\rangle$$

$$=\left\langle-\boldsymbol{u}'\cdot\boldsymbol{U}\times\boldsymbol{\omega}'\right\rangle+\left\langle\boldsymbol{u}'\cdot\boldsymbol{U}\times\boldsymbol{\omega}'\right\rangle=0 \tag{21}$$

Flow turning has now vanished identically; a result, we must add, that fully agrees with experimental evidence and other formal analyses.[58-60] For example, Van Moorhem[60] had proven, in his rigorous mathematical treatment of the problem, that flow turning could not exist in *any* three-dimensional setting, albeit omnipresent in one-dimensional analysis.

This correction alone leads to major improvement in reaching an agreement with experimental data. The lesson here is that only by accounting for *all* unsteady energy gains and losses that a correct linear stability theory can be achieved. Other terms in Eq. (18) once thought to have important stability implications do not appear when the integrals are rearranged, combined and evaluated.

We have recently completed a full evaluation of Eq. (18) for the solid motor case; current efforts are focused on a similar evaluation for the liquid engine problem. This has already been carried out for longitudinal waves (initial results are described in a companion paper[51]); major effort is now being devoted to the transverse mode case of central importance to large engine development programs.

F. Effects of Nonlinearity

It is now required to examine nonlinear terms arising from the expansion of Eq. (13). The most significant of these are the energy losses incurred in steep wave fronts. To do so, one must focus on the last set of terms in Eq. (13). After temporal and spatial averaging, one is left with

$$\iiint_V\left\langle\frac{\delta^2}{(\gamma-1)Pr}\nabla^2T+\delta_d^2\left(\nabla\cdot\boldsymbol{u}\right)^2\right\rangle\mathrm{d}V \tag{22}$$

Those readers familiar with gasdynamics will recognize in this term the source of the entropy gain and associated energy loss in a steep wave front. In fact, this term is usually ignored because it is only meaningful when there are very steep gradients in particle velocity and temperature. Here we proceed to evaluate this term by considering a very small portion of the chamber volume that encompasses the shock layer corresponding to a steepened wave system as described earlier. The shock layer can be treated as a region of nonuniformity, as clearly illustrated in Fig. 6.

Following standard procedures, Eq. (22) can be reduced to the classical textbook result showing the origin of the entropy gain in the shock wave. By manipulations using the Rankine-Hugoniot equations, we find the formula for the energy loss in the steep wave to be

$$\left(\frac{\mathrm{d}E}{\mathrm{d}t}\right)_{\text{shock}}=-\frac{S_{\text{port}}}{\gamma(\gamma-1)}\frac{(s_2-s_1)^*}{c_v}$$

$$=-\left(\frac{\varepsilon_{\text{shock}}}{\bar{P}}\right)^3 S_{\text{port}}\left(\frac{\gamma+1}{12\gamma^3}\right) \tag{23}$$

leading to a simple approximation for the nonlinear stability parameter in Eq. (17), namely

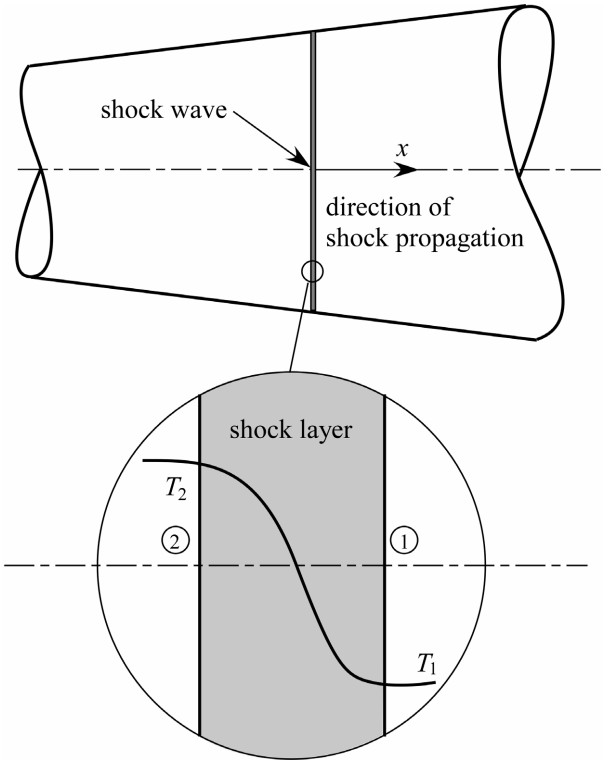

Fig. 6 Shock layer structure.

$$\alpha^{(2)} = -\frac{(\gamma+1)}{3E^2}\left(\frac{\xi}{2\gamma}\right)^3 S_{\text{port}} \qquad (24)$$

Here ξ is a factor dependent upon the assumed waveform for the traveling shock wave, and S_{port} is the area of the shock front. In the longitudinal case, this is simply the cross-sectional area of the duct at a convenient location.

This nonlinear loss effect is the principal damping mechanism in both liquid and solid propellant motors, and is the key element in understanding the limit cycle behavior so often encountered when finite amplitude waves appear. It is tempting to carry the implied perturbation series in Eq. (17) to higher than second order in the system amplitude. However, this is not justified in the present situation because we assume that the unsteady flowfield and mode shape information for the chamber are accurate only to the first order in wave amplitude. Having provided a consistent formulation, it may be useful to test the results that we have obtained against experimental evidence.

G. Limit Cycle Amplitude

In liquid propellant engines, one is seldom interested in tracing the details of the growth of the waves to their final state. Such engines usually operate for very long time on the time scale of the wave motions, with very slow changes in the steady operating parameters. For this reason, strictly linear models provide no useful information in the predictive sense. There is, however, a well-known rule of thumb suggesting that large values of the linear growth rate, $\alpha^{(1)}$, estimated from Eq. (18), correlate with large values of the limit cycle amplitude. Clearly, it is the latter amplitude that is of concern, since it is a measure of the vibration and other impacts on the system due to the oscillations.

What is required is information concerning the limit amplitude reached as the wave system approaches a fully steepened form. Equation (17) provides the required limit amplitude. In the fully steepened state, the wave amplitude is stationary, and it may be readily seen that the limit amplitude is

$$\varepsilon_{\text{limit}} = -\alpha^{(1)} / \alpha^{(2)} \qquad (25)$$

Evidently, the outcome will be physically meaningful only when $\alpha^{(2)}$ is negative. This will always be the case for the shock loss mechanism described by Eq. (24). Recently, Eq. (25) has been tested for many solid rocket data sets and has been found to yield an excellent estimate of their limiting amplitudes. At this juncture, it may be worthwhile to reiterate the fact that accurate results are not possible without a valid linear stability base.

H. Triggering Amplitude

For many years now, this calculation has led to many controversial arguments. If one examines Fig. 5, particularly, in the context of Eq. (17) (with extension to higher orders in the wave amplitude), it may be readily seen that it is theoretically possible to raise the amplitude of a system oscillating at its lowest limit amplitude to a yet higher limit amplitude; this can be accomplished, for example, by adding sufficient energy in a pulse to raise the oscillations above a critical triggering level (see figure). This mechanism is what might be termed *true triggering*. Careful examination of solid rocket data shows that this scenario seldom fits what is actually observed. In every case studied by the authors, motors that exhibited "triggering" were linearly unstable motors. That is, they are not stable motors that are *triggered* into a high-amplitude limit cycle. When such motors operate without deliberate pulsing, the wave system grows so slowly from the random noise that is always present, that oscillations are barely measurable by the end of the burn. However, when the motor is disturbed by a sufficiently large pulse, the broadband energy increment excites finite amplitude steep fronted waves. The system then grows rapidly to the limit cycle amplitude. Calculations using Eq. (25) agree very well with actual observations. We believe that true triggering is seldom, if ever, observed in actual rocket motors. Much of the confusion over this issue has resulted from application of faulty predictive codes that almost always predict a linearly stable system. A classic example can be found in the recent experiments by Blomshield.[61] Every motor fired in this test series was predicted by the SSP to be linearly stable. In fact many of the motors were linearly unstable at least during part of the burn. Unless pulsed, only very low level oscillations were present. Sufficiently strong pulsing during linearly unstable operation led to violent oscillations in several tests.

IV. Application to Liquid Engines

We have recently used the model described in this paper in the analysis of longitudinal mode oscillations of liquid propellant engine preburners. Preliminary findings are reported in a companion paper.[51] As in the case of the solid motor application, predictive capability is very promising and the results compare favorably to measurements.

In applying the results to large liquid rockets with potential transverse mode instability, considerable work remains to be accomplished. In particular, it is necessary to treat the three-dimensional coupling between the waves and the combustion heat release. The first step is to establish that steep waves can be

formed in the transverse mode case. The information submitted in Part II of this paper strongly suggests that steep-fronted wave do represent an important feature of high-amplitude transverse mode instability of liquid rocket combustion.

Another aspect of the problem requiring attention is the application of detonation wave physics to the combustion model in the present situation. Clearly, shock motions in the unreacted injection mixture may have a large impact on the energy transfer from combusion to the wave system.

It remains to be demonstrated that a simple model of the type used in the longitudinal case (see Eq. (1)) is valid for transverse modes. It is essential to recognize that the use of method of characteristics or full Navier-Stokes CFD algorithms will be futile in seriously attempting to solve this problem. What is needed is a simple model that can rapidly and accurately determine the system stability characteristics without the expense and time required in a strictly numerical attack on the problem. This is not to say that there is not a future role for CFD in the solution of combustion instability problems. However, a crucial first step is to perfect a simple predictive algorithm based on concepts such as those developed in this paper. The subcomponents could then be refined, discretized, and resolved using multiple numerical modules.

A crucial step is to simplify the mathematical description of the unsteady flowfield. It is possible to utilize a three-dimensional form of Eq. (1) to represent a steep fronted traveling tangential mode; Bessel function mode shapes are then required. Figure 7 is a frame from an animation of calculations describing a steep wave front formed by superimposing a set of standing tangential modes. Twenty modes were used to produce the surface shown. The traveling shock wave traverses the chamber once every period of the first tangential mode. This representation of the unsteady flow is in excellent agreement with what is described in the F-1 data and in Clayton's known measurements.

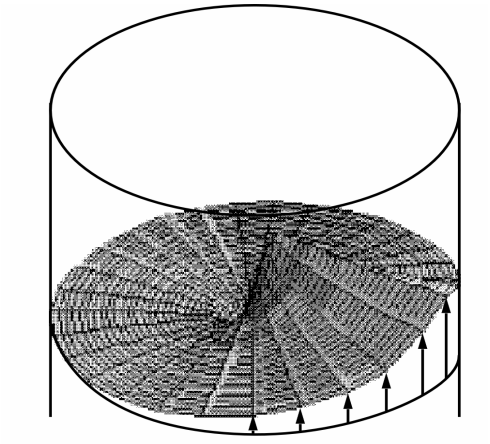

Fig. 7 Traveling tangential shock wave (simulated).

These findings are contrary to accepted ideas, which hold that transverse modes cannot steepen even though very large amplitudes might be present. The classical work of Maslen and Moore is often cited as proof of this idea.[52] However, this view does not agree with much experimental data that tends to suggest otherwise.

Finally, it should be observed that a high-amplitude steep wave front traveling across the injector face will have major impact on heat transfer rates and on transverse forces acting on surface structures. The authors have identified this mechanism to be responsible for severe injector damage often associated with finite amplitude combustion oscillations.

Acknowledgments

This work was sponsored partly by the University of Tennessee, UTSI, and partly by the NASA Marshall Spaceflight Center, under Grant No. NNM04AA30G, Technical Officer, J. D. Sims. The first author wishes to express appreciation for additional support from the Edward J. and Carolyn P. Boling Chair of Excellence in Advanced Propulsion, University of Tennessee.

References

[1]Crocco, L., and Cheng, S. I., "Theory of Combustion Instability in Liquid Propellant Rocket Motors," *AGARD*, Vol. 8, Butterworths Sci. Pub. Ltd, London, UK, 1956.

[2]Culick, F. E. C., "High Frequency Oscillations in Liquid Rockets," *AIAA Journal,* Vol. 1, No. 5, 1963, pp. 1097-1104.

[3]Culick, F. E. C., and Yang, V., "Overview of Combustion Instabilities in Liquid Propellant Rocket Engines," *Liquid Rocket Engine Combustion Instability*, Vol. 169, edited by V. Yang and W. E. Anderson, AIAA Progress in Astronautics and Aeronautics, 1995, pp. 1-37.

[4]Culick, F. E. C., "A Note on Rayleigh's Criterion," *Combustion Science and Technology,* Vol. 56, 1987, pp. 159-166.

[5]Harrje, D. T., and Reardon, F. H., "Liquid Propellant Rocket Combustion Instability," NASA, Technical Rept. SP-194, July 1972.

[6]Sirignano, W. A., and Crocco, L., "A Shock Wave Model of Unstable Rocket Combustion," *AIAA Journal,* Vol. 2, No. 7, 1964.

[7]Zinn, B. T., "A Theoretical Study of Nonlinear Combustion Instablity in Liquid Propellant Engines," *AIAA Journal,* Vol. 6, No. 10, 1968, pp. 1966-1972.

[8]Flandro, G. A., "Analysis of Nonlinear Combustion Instability," SIAM Minisymposium, March 1998.

[9]Flandro, G. A., "Nonlinear Unsteady Solid Propellant Flame Zone Analysis," AIAA Paper 98-3700, 1998.

[10]Flandro, G. A., "Effects of Vorticity on Rocket Combustion Stability," *Journal of Propulsion and Power,* Vol. 11, No. 4, 1995, pp. 607-625.

[11]Flandro, G. A., and Majdalani, J., "Aeroacoustic Instability in Rockets," *AIAA Journal,* Vol. 41, No. 3, 2003, pp. 485-497.

[12]Flandro, G. A., Majdalani, J., and French, J. C., "Incorporation of Nonlinear Capabilities in the Standard Stability Prediction Program," AIAA Paper 2004-4182, July 2004.

[13]Flandro, G. A., Majdalani, J., and French, J. C., "Nonlinear Rocket Motor Stability Prediction: Limit Amplitude, Triggering, and Mean Pressure Shift," AIAA Paper 2004-4054, July 2004.

[14]Sotter, J. G., Woodward, J. W., and Clayton, R. M., "Injector Response to Strong High-Frequency Pressure Oscillations," *Journal of Spacecraft and Rockets,* Vol. 6, No. 4, 1969, pp. 504-506.

[15]Sotter, J. G., and Clayton, R. M., "Monitoring the Combustion Process in Large Engines," *Journal of Spacecraft and Rockets,* Vol. 4, No. 5, 1967, pp. 702-703.

[16]Clayton, R. M., "Experimental Measurements on Totating Detonation-Like Combustion," JPL, Technical Rept. 32-788, Pasadena, CA, August 1965.

[17]Clayton, R. M., Rogero, R. S., and Sotter, J. G., "An Experimental Description of Destructive Liquid Rocket Resonant Combustion," *AIAA Journal,* Vol. 6, No. 7, 1968, pp. 1252-1259.

[18]Culick, F. E. C., "Combustion Instabilities in Propulsion Systems," *Unsteady Combustion*, Kluwer Academic Publishers, 1996, pp. 173-241.

[19]Culick, F. E. C., "Stability of Three-Dimensional Motions in a Rocket Motor," *Combustion Science and Technology,* Vol. 10, No. 3, 1974, pp. 109-124.

[20]Culick, F. E. C., "The Stability of One-Dimensional Motions in a Rocket Motor," *Combustion Science and Technology,* Vol. 7, No. 4, 1973, pp. 165-175.

[21]Culick, F. E. C., "Nonlinear Behavior of Acoustic Waves in Combustion Chambers," California Institute of Technology, Pasadena, CA, July 1975.

[22]Culick, F. E. C., and Yang, V., "Prediction of the Stability of Unsteady Motions in Solid Propellant Rocket Motors," *Nonsteady Burning and Combustion Stability of Solid Propellants*, Vol. 143, edited by L. De Luca, E. W. Price, and M. Summerfield, AIAA Progress in Astronautics and Aeronautics, Washington, DC, 1992, pp. 719-779.

[23]Culick, F. E. C., "Acoustic Oscillations in Solid Propellant Rocket Chambers," *Acta Astronautica,* Vol. 12, No. 2, 1966, pp. 113-126.

[24]Culick, F. E. C., "Rotational Axisymmetric Mean Flow and Damping of Acoustic Waves in a Solid Propellant Rocket," *AIAA Journal,* Vol. 4, No. 8, 1966, pp. 1462-1464.

[25]Culick, F. E. C., "Stability of Longitudinal Oscillations with Pressure and Velocity Coupling in a Solid Propellant Rocket," *Combustion Science and Technology,* Vol. 2, No. 4, 1970, pp. 179-201.

[26]Lovine, R. L., Dudley, D. P., and Waugh, R. D., "Standardized Stability Prediction Method for Solid Rocket Motors," Aerojet Solid Propulsion Co., Vols. I, II, III Rept. AFRPL TR 76-32, CA, May 1976.

[27]Nickerson, G. R., Culick, F. E. C., and Dang, L. G., "Standardized Stability Prediction Method for Solid Rocket Motors Axial Mode Computer Program," Software and Engineering Associates, Inc., AFRPL TR-83-017, September 1983.

[28]Flandro, G. A., "On Flow Turning," AIAA Paper 95-2530, July 1995.

[29]Flandro, G. A., Cai, W., and Yang, V., "Turbulent Transport in Rocket Motor Unsteady Flowfield," *Solid Propellant Chemistry, Combustion, and Motor Interior Ballistics*, Vol. 185, edited by V. Yang, T. B. Brill, and W.-Z. Ren, AIAA Progress in Astronautics and Aeronautics, Washington, DC, 2000, pp. 837-858.

[30]Majdalani, J., Flandro, G. A., and Roh, T. S., "Convergence of Two Flowfield Models Predicting a Destabilizing Agent in Rocket Combustion," *Journal of Propulsion and Power,* Vol. 16, No. 3, 2000, pp. 492-497.

[31]Majdalani, J., and Van Moorhem, W. K., "Improved Time-Dependent Flowfield Solution for Solid Rocket Motors," *AIAA Journal,* Vol. 36, No. 2, 1998, pp. 241-248.

[32]Majdalani, J., "The Boundary Layer Structure in Cylindrical Rocket Motors," *AIAA Journal,* Vol. 37, No. 4, 1999, pp. 505-508.

[33]Majdalani, J., "Vorticity Dynamics in Isobarically Closed Porous Channels. Part I: Standard Perturbations," *Journal of Propulsion and Power,* Vol. 17, No. 2, 2001, pp. 355-362.

[34]Majdalani, J., and Roh, T. S., "Vorticity Dynamics in Isobarically Closed Porous Channels. Part II: Space-Reductive Perturbations," *Journal of Propulsion and Power,* Vol. 17, No. 2, 2001, pp. 363-370.

[35]Majdalani, J., and Roh, T. S., "The Oscillatory Channel Flow with Large Wall Injection," *Proceedings of the Royal Society, Series A,* Vol. 456, No. 1999, 2000, pp. 1625-1657.

[36]Vuillot, F., and Avalon, G., "Acoustic Boundary Layer in Large Solid Propellant Rocket Motors Using Navier-Stokes Equations," *Journal of Propulsion and Power,* Vol. 7, No. 2, 1991, pp. 231-239.

[37]Roh, T. S., Tseng, I. S., and Yang, V., "Effects of Acoustic Oscillations on Flame Dynamics of Homogeneous Propellants in Rocket Motors," *Journal of Propulsion and Power,* Vol. 11, No. 4, 1995, pp. 640-650.

[38]Yang, V., and Roh, T. S., "Transient Combustion Response of Solid Propellant to Acoustic Disturbance in Rocket Motors," AIAA Paper 95-0602, January 1995.

[39]Vuillot, F., "Numerical Computation of Acoustic Boundary Layers in Large Solid Propellant Space Booster," AIAA Paper 91-0206, January 1991.

[40]Baum, J. D., Levine, J. N., and Lovine, R. L., "Pulsed Instabilities in Rocket Motors: A Comparison between Predictions and Experiments," *Journal of Propulsion and Power,* Vol. 4, No. 4, 1988, pp. 308-316.

[41]Baum, J. D., "Investigation of Flow Turning Phenomenon; Effects of Frequency and Blowing Rate," AIAA Paper 89-0297, January 1989.

[42]Glick, R. L., and Renie, J. P., "On the Nonsteady Flowfield in Solid Rocket Motors," AIAA Paper 84-1475, June 1984.

[43]Brown, R. S., Blackner, A. M., Willoughby, P. G., and Dunlap, R., "Coupling between Acoustic Velocity Oscillations and Solid Propellant Combustion," *Journal of Propulsion and Power,* Vol. 2, No. 5, 1986, pp. 428-437.

[44]Shaeffer, C. W., and Brown, R. S., "Oscillatory Internal Flow Field Studies," United Technologies, AFOSR Contract Rept. F04620-90-C-0032, San Jose, CA, August 1990.

[45]Shaeffer, C. W., and Brown, R. S., "Oscillatory Internal Flow Studies," United Technologies, Chemical Systems Div. Rept. 2060 FR, San Jose, CA, August 1992.

[46]Cantrell, R. H., and Hart, R. W., "Interaction between Sound and Flow in Acoustic Cavities: Mass, Momentum, and Energy Considerations," *Journal of the Acoustical Society of America,* Vol. 36, No. 4, 1964, pp. 697-706.

[47]Brownlee, W. G., "Nonlinear Axial Combustion Instability in Solid Propellant Motors," *AIAA Journal,* Vol. 2, No. 2, 1964, pp. 275-284.

[48]Flandro, G. A., "Approximate Analysis of Nonlinear Instability with Shock Waves," AIAA Paper 82-1220, July 1982.

[49]Flandro, G. A., "Energy Balance Analysis of Nonlinear Combustion Instability," *Journal of Propulsion and Power,* Vol. 1, No. 3, 1985, pp. 210-221.

[50]Levine, J. N., and Baum, J. D., "A Numerical Study of Nonlinear Phenomena in Solid Rocket Motors," *AIAA Journal,* Vol. 21, No. 4, 1983, pp. 557-564.

[51]Flandro, G. A., Majdalani, J., and Sims, J. D., "Nonlinear Longitudinal Mode Instability in Liquid Propellant Rocket Engine Preburner," AIAA Paper 2004-4162, July 2004.

[52]Maslen, S. H., and Moore, F. K., "On Strong Transverse Waves without Shocks in a Circularcylinder," *Journal of the Aeronautical Sciences,* Vol. 23, 1956, pp. 583-593.

[53]Oefelein, J. C., and Yang, V., "Comprehensive Review of Liquid-Propellant Combustion Instabilities in F-1 Engines," *Journal of Propulsion and Power,* Vol. 9, No. 5, 1993, pp. 657-677.

[54]Flandro, G. A., and Sotter, J. G., "Unstable Combustion in Rockets," *Scientific American*, 1968.

[55]Culick, F. E. C., "Non-Linear Growth and Limiting Amplitude of Acoustic Oscillations in Combustion Chambers," *Combustion Science and Technology,* Vol. 3, No. 1, 1971, pp. 1-16.

[56]Kirchoff, G., *Vorlesungen Über Mathematische Physik: Mechanik*, 2nd ed., Teubner, Leibzig, 1877, pp. 311-336.

[57]Flandro, G. A., and Roach, R. L., "Effects of Vorticity Production on Acoustic Waves in a Solid Propellant Rocket," Air Force Office of Scientific Research, AFOSR Final Rept. 2060 FR, Bolling AFB, DC, October 1992.

[58]Malhotra, S., "On Combustion Instability in Solid Rocket Motors," Dissertation, California Institute of Technology, 2004.

[59]Van Moorhem, W. K., "An Investigation of the Origin of the Flow Turning Effect in Combustion Instability," 17th JANNAF Combustion Conference, September 1980.

[60]Van Moorhem, W. K., "Flow Turning in Solid-Propellant Rocket Combustion Stability Analyses," *AIAA Journal,* Vol. 20, No. 10, 1982, pp. 1420-1425.

[61]Blomshield, F. S., "Stability Testing and Pulsing of Full Scale Tactical Motors, Parts I and II," Naval Air Warfare Center, NAWCWPNS TP 8060, February 1996.